Real-Time Electrochemical Impedance Spectroscopy Diagnosis of the Marine Solid Oxide Fuel Cell

Hironori Nakajima and Tatsumi Kitahara

Department of Mechanical Engineering, Faculty of Engineering, Kyushu University, 744 Motooka, Nishi-ku, Fukuoka 819-0395, Japan

E-mail: nakajima@mech.kyushu-u.ac.jp

Abstract. We have investigated the behavior of an operating solid oxide fuel cell (SOFC) with supplying a simulated syngas to develop SOFC diagnosis method for marine SOFC units fueled with liquefied natural gas. We analyse the characteristics of syngas fueled anode of an intermediate temperature microtubular SOFC at 500 °C as a model case by electrochemical impedance spectroscopy (EIS) to find parameters useful for the diagnosis. EIS analyses are performed with an equivalent circuit model consisting of several resistances and capacitances attributed to the anode and cathode processes. The characteristic changes of those circuit parameters by internal reforming and anode degradation show that they can be used for the real-time diagnosis of operating SOFCs.

1. Introduction

The adoption of the liquefied natural gas (LNG) fueled solid oxide fuel cell (SOFC) to the marine power supplies and motive powers is expected to reduce fuel consumption and toxic air pollutant (NO_x, SO_x, Particulate Matter (PM), CO_2) emissions compared with the conventional marine diesel engine [1–8]. The SOFC achieves high efficiency power generation owing to the high temperature operation at 600-1000 °C. The SOFC is also comparatively tolerant of the use of hydrocarbon fuel such as the natural gas. In the near future, SOFC-diesel hybrid motive power would be promising as the marine use where the SOFC power units operate as auxiliary power unit (APU) for the steady power demand, while the diesel engine responds to the load change (Fig. 1). SOFC-micro gas turbine combined units as illustrated in Fig. 2 for the marine use can be developed by scaling-up a combined system under demonstration [9, 10].

We thus focus on the development of real-time abnormal-diagnosis method to improve the reliability and durability required for the long-term safety and stable operation of the marine SOFC. Significant accident due to the breakdown of the cell should also be prevented. We therefore apply electrochemical impedance spectroscopy (EIS) [11, 12] to the diagnosis which enables safety precautions, operating condition modification, and emergency shutdown by prior abnormality detection of the SOFC through an elucidation of the degradation factor accompanying the marine operation.

EIS has been broadly used for the analysis of fuel cells. In particular, we have so far modeled a polymer electrolyte fuel cell (PEFC) and an SOFC with electric equivalent circuits constituted by resistances and capacitances to develop the diagnosis method analyzing the variation of each resistance and capacitance [13, 14]. This diagnosis clarifies the operational status of the cells

and the voltage losses by internal resistances associated with several processes. There have been a number of EIS studies on SOFCs aiming at characterization and evaluation of the developed anode (fuel electrode) and the cathode (air electrode) materials. However, very few papers analyze each impedance of the anode and cathode in full cell impedance spectra of a practical cell simultaneously and separately by applying EIS under operation [14]. Moreover, researches connected to the abnormal-diagnosis method using such full cell impedance spectra have not been reported.

We therefore carry out EIS with a two electrode setup on a practical microtubular SOFC, which can be operated in the intermediate temperature range of 500-800 °C(IT-SOFC), as a model case. To evaluate the impedance variation of each part of the cell under operation, the gas-feed condition for the anode was varied.

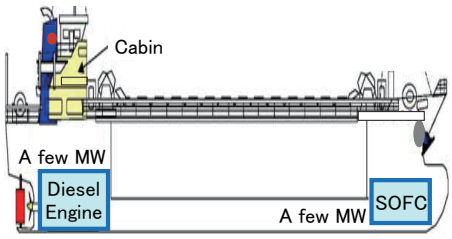

Figure 1. Concept of the SOFC-Diesel Hybrid Ship.

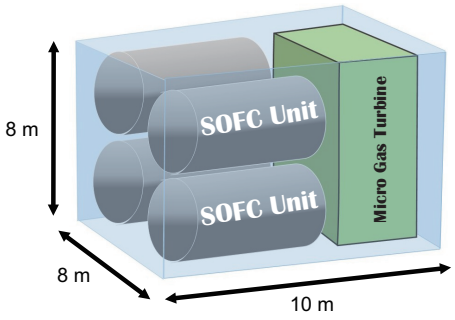

Figure 2. SOFC units combined with a micro gas turbine.

2. Experimental

All measurements were performed using an anode-supported microtubular SOFC [15–17] with an outer and an inner diameters of 10 mm and 7 mm, respectively. The thickness of the electrolyte was 30 μm. Anode substrate tube was made of NiO/$(ZrO_2)_{0.9}(Y_2O_3)_{0.1}$(NiO/YSZ). Anode interlayer of NiO/$(Ce_{0.9}Gd_{0.1})O_{1.95}$ (NiO/GDC10) for low temperature operation was coated onto the anode substrate. Electrolyte was $La_{0.8}Sr_{0.2}Ga_{0.8}Mg_{0.2}O_{2.8}$(LSGM). A layer of $(Ce_{0.6}La_{0.4})O_{1.8}$ (LDC40) was inserted between the anode interlayer and electrolyte to prevent undesirable nickel diffusion during cell preparation at high temperature. Cathode made of $(La_{0.6}Sr_{0.4})(Co_{0.2}Fe_{0.8})O_3$(LSCF) was coated on the electrolyte. Geometrical electrode area was 24.2 cm^2.

Figure 3 illustrates the configuration of the experimental set-up. Temperature of the cell at open circuit voltage was maintained at 500 °C with a tubular electric furnace so that the degradation by the internal reforming reaction of methane becomes remarkable under low temperature for the test. Anode gas line was supplied with mixtures of H_2/N_2 or the simulated syngas at a constant flow rate. The simulated syngas composition was determined from the assumption of a methane fed reformer temperature of 500 °C and a steam/carbon ratio of 2 at the reformer inlet. The cell inlet flow rates are presented in Table 1. Cathode gas line was supplied with dry air at a constant flow rate of 2000 cm^3 min^{-1}. The anode NiO was reduced to Ni by feeding H_2/N_2 mixture gas for two hours prior to measurements. The anode and cathode were electrically connected with the four-terminal method.

Current-voltage (I-V) curves were measured with an electrical load (PLZ164WA, Kikusui Co Ltd) and mass flow controllers (SEC-E40MK3, Horiba STEC) controlled by LabView 8.6 (National Instruments Inc.) on a personal computer. ElS measurements were carried out using a

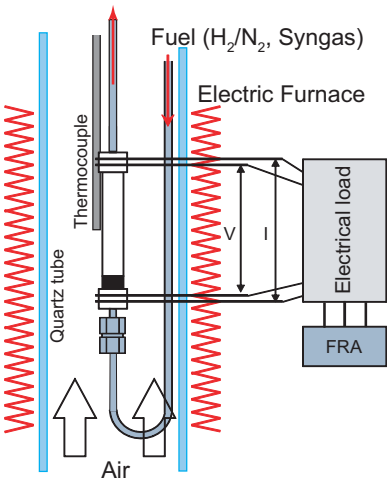

Figure 3. Experimental set-up of the microtubular SOFC.

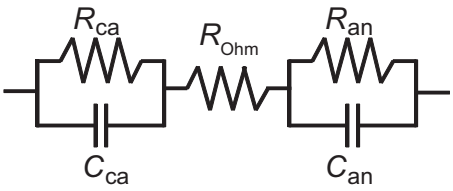

Figure 4. Equivalent circuit of an SOFC.

frequency response analyzer (FRA) (FRA 5022, NF Co Ltd.) combined with the electrical load. EIS was carried out with two-electrode set-up without the reference electrode. An equivalent circuit presented in Fig. 4 [12, 18] is used for the complex nonlinear least square (CNLS) fitting [12] of obtained impedance spectra with excluding inductive part.

Each resistance and capacitance is evaluated with a CNLS fitting program, Z-View (Scribner Inc.). In this circuit, R_{ca} and C_{ca} denote the cathode resistance and associated capacitance, respectively, R_{Ohm} is the Ohmic resistance of the cell, R_{an} and C_{an} are the anode resistance and associated capacitance, respectively.

Each one of the R-C branches dominantly represents the charge transfer process in low current density region, and mass transfer process in high current density region [14]. In the present paper, the equivalent circuit is not separated into the charge and mass transfer processes since our complex plane plots exhibited one arc for each of the anode and cathode processes, whose behavior should be analyzed with simple one R-C branch prior to appropriate separations of overlapping arcs and equivalent circuit.

The Nernst loss [19–22] by the partial pressure gradient of hydrogen and oxygen ascribed to their consumption leads to current distribution in the axial direction. Ohmic resistance in the anode and cathode electrodes is also attributed to this current distribution. However, we use the above equivalent circuit for uniform current distribution to obtain average behavior over the axial direction of the cell.

Table 1. Inlet gas flow rates for the H_2/N_2 and the simulated syngas fuels (cm^3min^{-1}).

	H_2	N_2	CO	CH_4	CO_2	H_2O
H_2/N_2	90	40	–	–	–	–
Syngas	90	–	4	35	22	121

3. Results and Discussion

3.1. I-V and EIS measurements

Figure 5 shows I-V curves recorded for hydrogen and simulated syngas fueled cell, where U_{ox} is an oxygen utilization. Each cell voltage decreases with switching from hydrogen to simulated syngas. The drop in the OCV indicates that the mixed potential ascribed to the redox potentials of muitiple species including hydrogen, water, carbon monoxide, carbon dioxide, methane, and carbon [23].

Figure 6 shows I-V curves recorded for hydrogen before and after the simulated syngas operation by I-V sweep cycles for 48 h. The cell voltage drop after the simulated syngas operation increases with the increase in the current density, while the OCV drop is small.

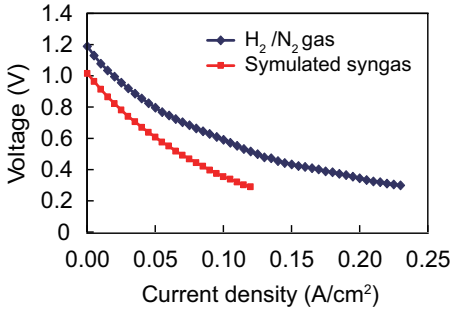

Figure 5. I-V curves of the SOFC with the H_2/N_2 or the simulated syngas fuels at 500 °C. Cathode: Dried air of 2000 cm^3min^{-1}. U_{ox} = 2.3% at 0.1 A cm^{-2}.

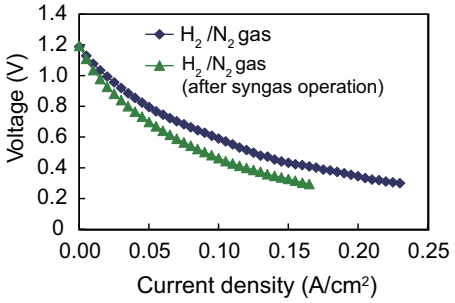

Figure 6. I-V curves of the SOFC supplied with the H_2/N_2 fuel at 500 °C. Cathode: Dried air of 2000 cm^3min^{-1}. U_{ox} = 2.3% at 0.1 A cm^{-2}.

Figure 7 presents impedance spectra (complex plane plots) for the hydrogen and simulated syngas operations. In the complex plane plots, semicircles are observed. The Ohmic resistance indicated at the high frequency intercept clearly appears to increase with the syngas operation by the I-V sweep cycles for 48 h. The Ohmic resistance does not recover after switching from syngas to hydrogen. The diameters of the semicircles for the hydrogen and syngas operations decrease with the increase in the current density, indicating large contribution of the catalytic reaction described by the Butler-Volmer type relashioship [24]. Thus deteriorations in the electron conduction and the catalyst activation are observed in the present measurements.

The separation of the semicircles between the cathode and anode are not so clearly seen in contrast to the cases at 700°C [14] because the time constants for the cathode and anode processes probably become close as the cell temperature lowers, resulting in the further overlapping semicircles.

Fitting results for H_2/N_2 and syngas conditions using the equivalent circuit in Fig. 4 are presented in Figs. 8. Here, the cathode resistance, R_{ca} for H_2/N_2 fuel is applied to that for the syngas condition since the CNLS fitting for the cathode impedance was not reliable due to the overlapping semicircles, in particular for the syngas. In the syngas operations, Ohmic resistance further increases compared with the hydrogen operation, indicating a temperatures drop of a cell. This is presumed to originate in the endothermic reaction of the internal reforming of the extra methane. Moreover, the anode resistance with the simulated syngas operation is slightly lower since electrochemically active additional gas such as hydrogen and carbon monoxide increase by the internal reforming of methane. The anode capacitance tends to increase with the syngas possibly due to the pseudocapacitance attributed to adsorbed species [25, 26] during the internal reforming process.

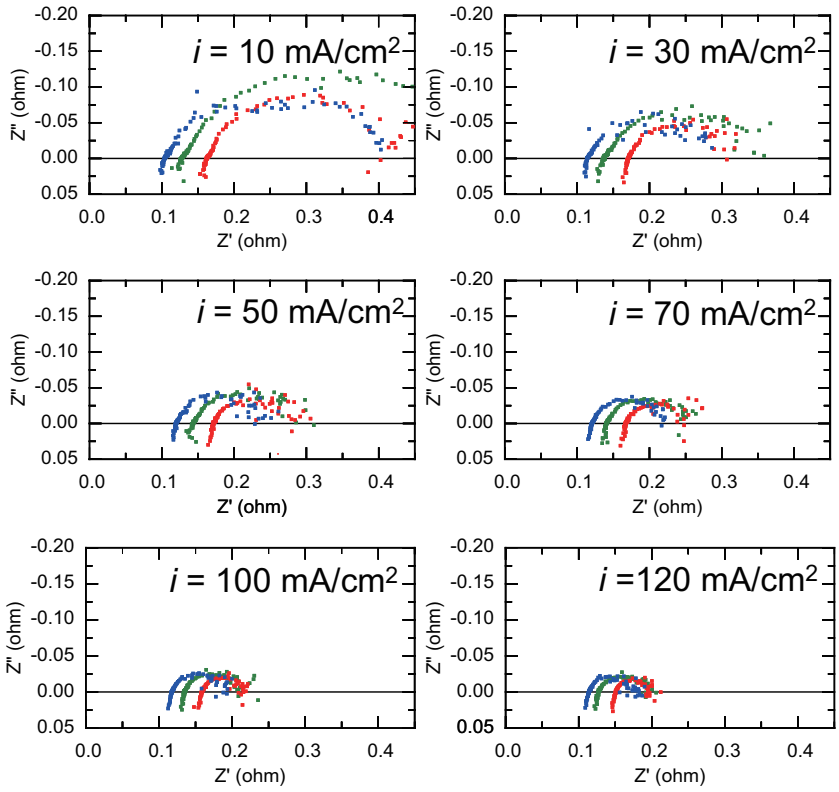

Figure 7. Complex-plane plots for the H_2/N_2 and simulated syngas fuels at different current densities, 500 °C. Cathode: Dried air of 2000 cm^3min^{-1}.

Fitting results for H_2/N_2 before and after the syngas operation are shown in Fig. 9. In comparison between those H_2/N_2 conditions, Ohmic resistance increases after the simulated syngas operation. Electronic conduction was possibly obstructed by network segmentation among the nickel catalyst particles by the stress associated with the carbon deposition. Moreover, the increase in the anode resistance indicates that the nickel catalyst activity deteriorates by the carbon deposition. The decrease in the anode capacitances is due to the decrease in the active area of the Ni catalyst by the segmented network and carbon deposition. The resistances and capacitances in the cathode side reasonably indicate small changes.

We extract the variations of the cell voltage and the resistances/capacitances indicated in Figs. 8 and 9 in addition to our previous paper for the cases of H_2/N_2 fuel [14] for the impedance diagnostic parameters as presented in Fig. 10. Each arrow indicates increase, decrease, or almost constant. When the oxygen partial pressure drops, the cell voltage becomes unstable. A diagnosis flow chart is thereby derived from the impedance variation as presented in Fig. 11.

4. Conclusion

We have clarified real-time quantitative diagnostic parameters under cell operation. For feasible major-accident prevention and emergency shutdown by abnormal detection/notification, and maintaining optimal operation, safety operation limits and performance sustainment limits are required to store in a database as reference threshold limits. Evaluation of the diagnostic parameters for the sulfur poisoning of the anode Ni catalyst [27, 28] from the fuel impurities and the cathode degradation by water vapor [29] and salty air [30] in the marine circumstance will be our future work.

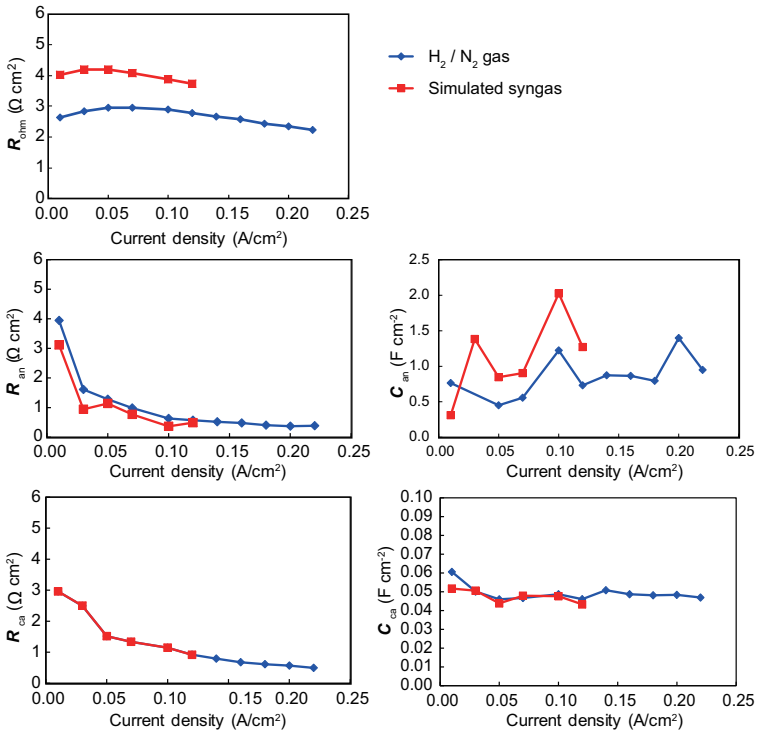

Figure 8. Equivalent circuit parameters of the SOFC fed with the H_2/N_2 or the simulated syngas fuels at 500 °C. Cathode : Dried air of 2000 cm^3min^{-1}.

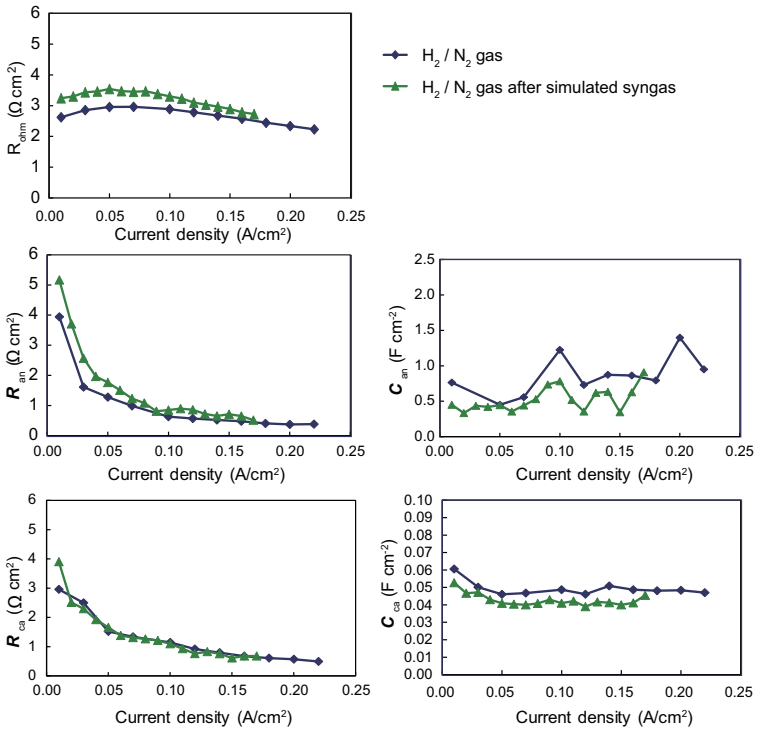

Figure 9. Equivalent circuit parameters of the SOFC fed with the H_2/N_2 before and after the simulated syngas operation at 500 °C. Cathode : Dried air of 2000 cm^3min^{-1}.

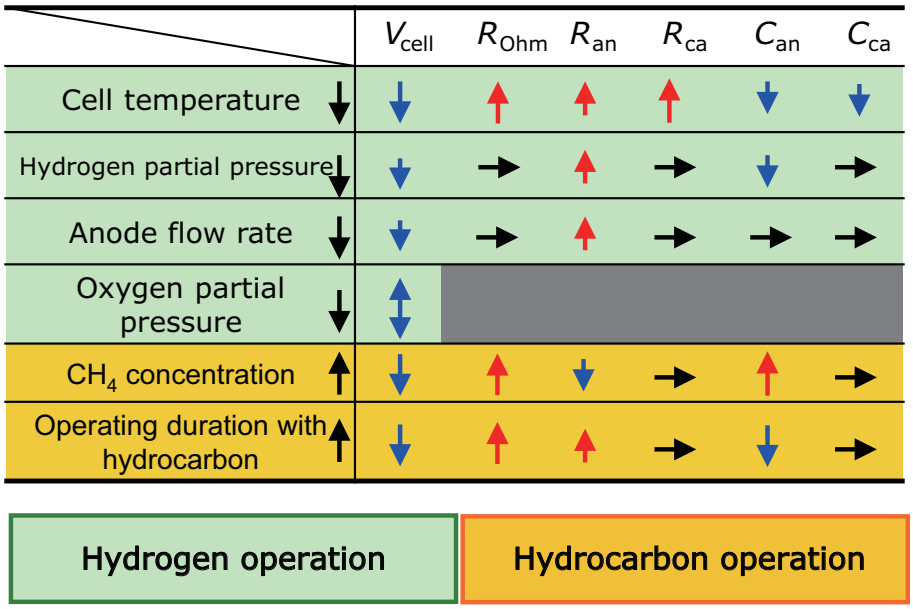

Figure 10. Variations of the cell voltage and the equivalent circuit parameters.

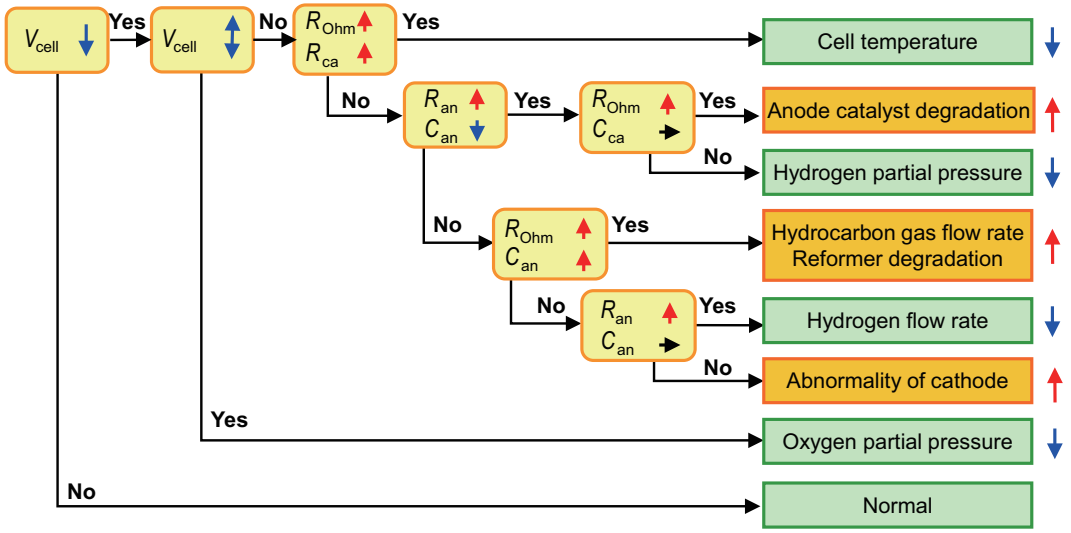

Figure 11. Diagnosis chart for the SOFC by the cell voltage and the equivalent circuit parameters.

Acknowledgments
Graduate students, Dr. Takuya Hoshiko (presently TOTO Co. Ltd.) and Mr. Jiro Hayashi (presently Toyota Motor Corporation) are gratefully acknowledged for assistance in the experiments.

References

[1] 2008 Marpol Annex VI International Maritime Organisation http://www.imo.org/en/OurWork/Environment/PollutionPrevention/AirPollution/Pages/Air-Pollution.aspx
[2] McConnell V P 2010 *Fuel Cells Bull.* **2010** 12 – 17
[3] Tse L K C, Wilkins S, McGlashan N, Urban B and Martinez-Botas R 2011 *J. Power Sources* **196** 3149 – 3162
[4] 2011 White paper roadmap to a single european transport area - towards a competitive and resource efficient transport system Official website of the European Union http://eur-lex.europa.eu/LexUriServ/LexUriServ.do?uri=COM:2011:0144:FIN:EN:PDF
[5] 2012 Directive 2012/33/EU of the European Parliament and of the Council Official website of the European Union http://eur-lex.europa.eu/legal-content/EN/TXT/PDF/?uri=CELEX:32012L0033&from=EN
[6] Welaya Y M A, Mosleh M and Ammar N R 2013 *Int. J. Nav. Archit. Ocean Eng.* **5** 529–545
[7] Welaya Y M A, Mosleh M and Ammar N R 2013 *J. Marine Sci. Appl.* **12** 473–483
[8] Díaz-de-Baldasano M C, Mateos F J, Núñez-Rivas L R and Leo T J 2014 *Appl. Energy* **116** 91 – 100
[9] 2014 *Fuel Cells Bull.* **2014** 1
[10] Kobayashi Y 2015 *Proceedings of the World Engineering Conference and Convention 2015* http://www.wfeo.org/wp-content/themes/wfeo/_mail/files/WECC2015_Proceedings/data/pdf/20284.pdf
[11] Bard A J and Faulkner L R 2001 *Electrochemical methods: Fundamentals and Applications* 2nd ed (New York: John Wiley & Sons)
[12] Barsoukov E and Macdonald J R (eds) 2005 *Impedance Spectroscopy: Theory, Experiment, and Applications* 2nd ed (New York: John Wiley & Sons)
[13] Nakajima H, Konomi T, Kitahara T and Tachibana H 2008 *J. Fuel Cell Sci. Technol.* **5** 041013
[14] Nakajima H, Kitahara T and Konomi T 2010 *J. Electrochem. Soc.* **157** B1686–B1692
[15] Kawakami A, Matsuoka S, Watanabe N, Saito T, Ueno A, Ishihara T, Sakai N and Yokokawa H 2006 *Ceram. Eng. Sci. Proc.* **27(4)** 3–13
[16] Watanabe N, Ooe T and Ishihara T 2012 *J. Power Sources* **199** 117 – 123
[17] Watanabe N, Ooe T, Akagi Y and Ishihara T 2012 *Int. J. Hydrogen Energy* **37** 8562 – 8571
[18] McIntosh S, Vohs J M and Gorte R J 2003 *J. Electrochem. Soc.* **150** A1305–A1312
[19] Morita H, Komoda M, Mugikura Y, Izaki Y, Watanabe T, Masuda Y and Matsuyama T 2002 *J. Power Sources* **112** 509–518
[20] Hemmes K 2004 *Modern Aspects of Electrochemistry* vol 37 ed White R, Conway B, Vayenas C and Gamboa-Adelco M (Kluwer Academic Publishers)
[21] Aydın Ö, Koshiyama T, Nakajima H and Kitahara T 2015 *J. Power Sources* **279** 218 – 223
[22] Aydın Ö, Nakajima H and Kitahara T 2015 *J. Power Sources* **293** 1053 – 1061
[23] Liu J and Barnett S A 2003 *Solid State Ionics* **158** 11 – 16
[24] Mizusaki J 2014 *Electrochemistry* **82** 819–829
[25] Hale J and Greef R 1967 *Electrochim. Acta* **12** 1409 – 1420
[26] Nakajima H, Nohira T, Ito Y, Kjelstrup S and Bedeaux D 2006 *J. Non-Equil. Thermody.* **31** 231–255
[27] Yokokawa H, Tu H, Iwanschitz B and Mai A 2008 *J. Power Sources* **182** 400 – 412
[28] Yoshizumi T, Taniguchi S, Shiratori Y and Sasaki K 2012 *J. Electrochem. Soc.* **159** F693–F701
[29] Liu R, Kim S, Taniguchi S, Oshima T, Shiratori Y, Ito K and Sasaki K 2011 *J. Power Sources* **196** 7090 – 7096
[30] Liu R R, Wang D J and Leng J 2013 *Chem. Res. Chin. Univ.* **29** 747–750